

Peclet number (α/L , where L is travel distance), was most strongly dependent on variance of the aperture distribution. Models by Smith et al. (1987) predict that the effects of connectivity and tortuosity could lead to major differences in the values of effective apertures derived from flow and tracer measurements. Such discrepancies have been observed in laboratory tests performed by Gale (1990) and Piggot and Elsworth (1990).

Piggot and Elsworth (1990) also performed tracer tests on fractures in a sheared condition. Although the fracture void volume was greater, the shape of the breakthrough curve was very similar to that obtained with the fracture in the mated condition.

Additional work is needed to more quantitatively relate geometrical properties of the void space to transport properties. It is worth reemphasizing that the limited available data show a lack of correlation between effective apertures based on hydraulic flow and transport measurements.

TWO-PHASE IMMISCIBLE FLUID FLOW

In single-phase flow, fracture geometry at the aperture scale determines flow and transport characteristics. Under two-phase immiscible fluid flow conditions, phase geometry (i.e., the geometry that is saturated with each phase) in the fracture ultimately controls the permeability to each phase, fluid pressure/saturation relationships, and solute dispersion in each phase. Phase geometry in the fracture also influences flow and transport through the surrounding porous matrix blocks by affecting hydraulic contact between the blocks. Although two-phase flow in porous media has received much attention, study of two-phase flow in fractures has only recently begun. Pressure/saturation and permeability/saturation relationships have been explored numerically and, more recently, measured in transparent rough-walled fracture analogs where phase geometry can be observed. The major difference between two-phase immiscible flow in porous media and in fractures is the two-dimensional nature of the aperture network. This increases the importance of phase interference and trapping phenomena, as discussed below.

Static and Quasi-Static Conditions

Under static conditions, viscous forces do not influence phase pressure. Therefore, assuming thermodynamic equilibrium, phase geometry in a horizontal fracture will be controlled entirely by capillary forces. The nonwetting fluid will be found in large apertures and the wetting fluid in small ones. The Laplace-Young equation (e.g., Adamson, 1990) relating the surface tension, T , to the pressure jump, ∇P , across the curved fluid-fluid interface ∇P dictates which phase is present at a particular location as a function of phase pressure:

$$\nabla P = T \left(\frac{1}{r_1} + \frac{1}{r_2} \right), \quad (3.7)$$

where r_1 and r_2 are the two principal radii of curvature. For a fracture the first principal radius of curvature, r_1 , is taken normal to the plane of the fracture and is equal to $b/(2\cos \alpha)$, where b is the local aperture and α is the fluid/fluid/rock contact angle. Local in-plane curvature, r_2 , is assumed not to contact the rock surface and therefore is not constrained by a contact angle. In a random aperture field, assuming that curvature in the plane of the fracture is negligible and that the distribution of phases is not inhibited by lack of accessibility will lead to phase structure/pressure relationships conforming to a percolation process on a two-dimensional network, as introduced by Broadbent and Hammersley (1957). A variety of interesting results come from percolation theory, the most important being that the phase geometry is fractal and that a critical pressure exists where one phase forms an infinite connected cluster isolating the other phase (see Chapter 7 in Feder, 1988).

Numerical simulation of the percolation process on spatially correlated aperture networks has been used to evaluate phase structure as a function of pressure. Subsequent modeling of flow through each phase structure allows estimation of relative permeability as a function of pressure (Pruess and Tsang, 1990; Pyrak-Nolte et al., 1990a). These calculations indicate significant phase interference. That is, the sum of the wetting and nonwetting phase relative permeabilities is considerably less than 1 (see Figure 3.12). Results of percolation theory on a random network also show that anisotropy in the correlation lengths (i.e., distances

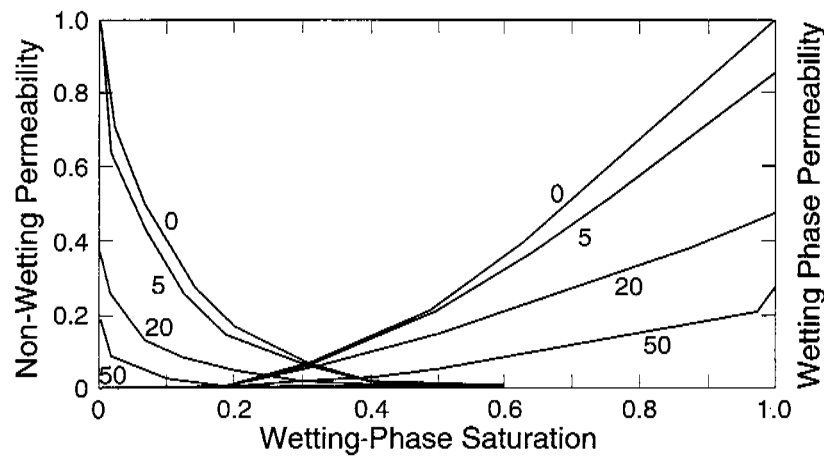


FIGURE 3.12 Effect of stress on relative permeabilities for a reduction in aperture of 5, 20, and 50 units of aperture. The saturation at which the nonwetting and wetting phase curves cross varies only a small amount with stress. From Pyrak-Nolte et al. (1990a).

over which similar values of a parameter are likely to be found) is required for the existence of two-phase mobility. This is because anisotropy can lead to the formation of parallel-connected phases. The validity of such methods for calculating two-phase fracture properties depends on the assumption that thermodynamic equilibrium predetermines phase structure for a given pressure and aperture structure. Equilibrium requires all apertures to be in a state of mutual communication. Three communication processes exist: (1) flow through the matrix that connects all apertures, (2) film flow along the fracture walls, and (3) diffusional processes. Recent experiments on a transparent cast of a natural fracture show that the interference between two phases flowing simultaneously in a fracture can be strong. At intermediate saturations, the sum of wetting and nonwetting phase-relative permeabilities was found to be much less than 1, supporting the results of numerical simulation (Persoff et al., 1991).

For a large number of situations, either communication processes do not exist or phase displacement occurs rapidly with respect to the communication processes. For these situations, accessibility of apertures to a phase (i.e., the proximity of an aperture to a phase and connection in the phase to a source or sink), places an additional control on phase geometry. If the displacement process is sufficiently slow that viscous forces can be neglected relative to capillary forces, accessibility rules may be combined with Eq. 3.7 to dictate the development of phase structure under quasi-static conditions.

Numerical models that incorporate the phase accessibility rule with Eq. 3.7, neglecting in-plane curvature, can be formulated; they conform to the process of invasion percolation introduced by Wilkinson and Willemsen (1983). Figure 3.13a shows the phase structure at breakthrough as water (the wetting fluid) supplied at the narrow boundary displaces air (the nonwetting fluid) under quasi-static conditions in a horizontal transparent rough-walled analog fracture. An example of a phase structure as simulated by the invasion percolation process on the measured aperture field for the experiment depicted in Figure 3.13a is shown in Figure 3.13b. The simulation predicts the phase structure to be much more complicated than what actually develops. Modification of the model to include in-plane curvature (r_2 in Eq. 3.7) in the calculation of aperture-phase entry pressure yields a phase structure (Figure 3.13c) comparable to those observed experimentally (Glass, 1993).

Processes by which a phase enters the fracture, including invasion from one edge of the fracture as discussed above, entry from the surrounding porous media, and entry through partitioning from the other phase, will significantly affect phase structure. As an example, Figure 3.14 shows the phase saturation structure in an air/water system in a horizontal analog fracture formed by a flat porous matrix in close contact with a roughened glass plate. Saturation/pressure relationships measured on this analog fracture/matrix system show strong hysteresis between wetting and drainage curves; nonwetting-phase entrapment reduced final wetting-phase saturation to approximately 60 percent (Glass and Norton, 1992).

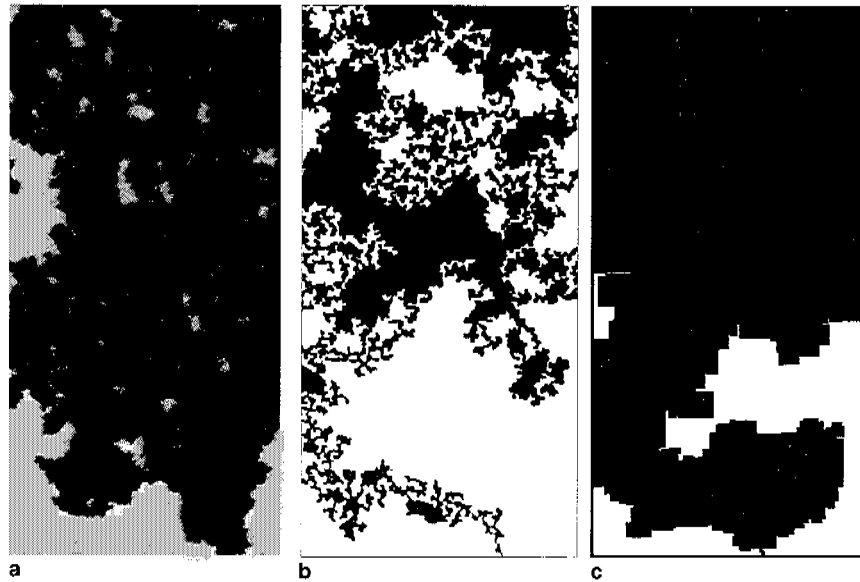


FIGURE 3.13 Phase structure at breakthrough in a rough-walled analog fracture with water (the wetting fluid, black) entry along the short side of the fracture (figure top) and air (white) exits along the other three sides of the fracture. Parts (a), (b), and (c) depict an experiment, a simulation using invasion percolation, and a simulation using a modified invasion percolation model, respectively. Simulations in parts *b* and *c* were carried out on the measured aperture field for the experiment a quarter of the size of that shown in part *a*. Gray areas in the simulation depict entrapped air phase. From Glass (1993).

For fractures that are nonhorizontal, gravity combines with capillarity under quasi-static conditions to dictate the sequence of fracture apertures that fill with the displacing phase. When the denser fluid underlies the lighter one, which is infiltrating from above, gravity tends to flatten the interface as displacement proceeds. However, if the more dense fluid is above the less dense fluid, gravity destabilizes the interface, resulting in the formation of gravity-driven fingers, even under quasi-static conditions. Experiments and simulations of gravity-driven fingering in the quasi-static limit show that the fingers widen and meander/branch as the inclination of the fracture with respect to the vertical decreases (Glass, 1993; Nicholl et al., 1993b). The opposite holds for fluids infiltrating from below. For example, air moving up into water-filled fractures will finger.

Dynamic Conditions

In situations where viscous forces are important, they combine with capillary, gravitational, and inertial forces (for large Reynolds numbers) to yield phase structure. In general, determination of the phase structure requires that the Navier-

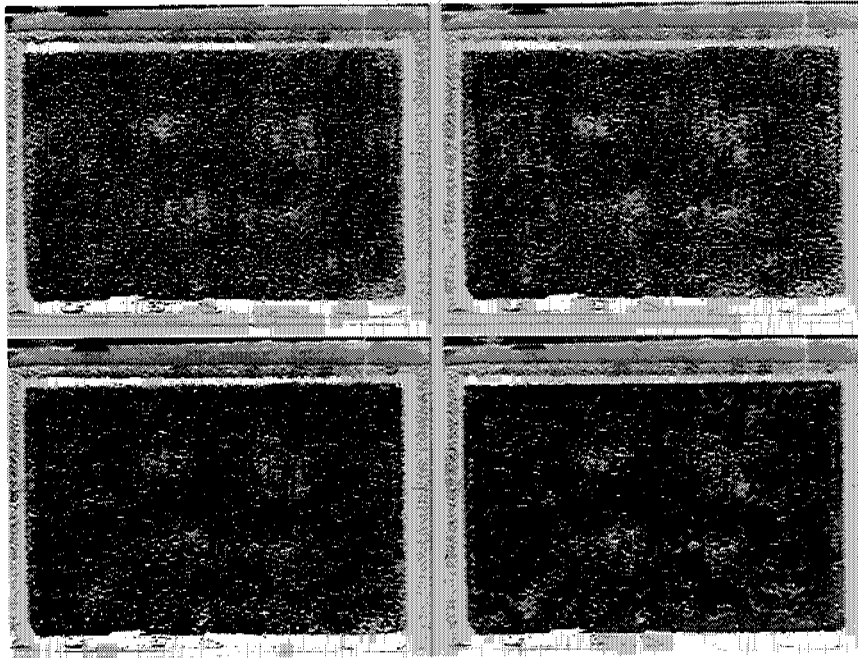


FIGURE 3.14 Growth of phase structure as a function of increasing liquid pressure (sequence is upper left, upper right, lower left, lower right) in an analog fracture/matrix system. Water (the wetting phase, black) enters the fracture from the saturated matrix. Air (the nonwetting phase, white) exits the fracture around the fracture edges. Courtesy of R. J. Glass.

Stokes equations for each fluid be solved with boundary conditions at the moving fluid/fluid interface incorporating a dynamic contact angle (Dussan, 1979; de Gennes, 1985). Although solution approaches based on cellular automata are under development (e.g., Stockman et al., 1990), this is still an intractable problem. Approaches that include accessibility rules and first-order viscous forces in the form of a modified invasion percolation model have been applied to porous networks and may be useful for fractures. Phase structures, however, may not be stable, and a variety of phenomena can occur, including viscous and gravity-driven fingering, flow pulsation, and blob flow (i.e., when one phase moves through another phase as a disconnected unit).

Viscous and gravity-driven fingering have been studied in smooth-walled fractures (Hele-Shaw cells) as an analog for two-phase flow in porous media. Linear stability analysis of the problem shows three factors to be influential in determining interfacial stability during a steady one-dimensional vertical downward displacement of one fluid (indicated by the subscript 2 below) by another (indicated by the subscript 1 below) in a smooth-walled fracture of aperture b :

(1) the fluid viscosity difference ($\mu_1 - \mu_2$), (2) the fluid density difference ($\rho_1 - \rho_2$), and (3) the interfacial velocity (U) (Saffman and Taylor, 1958; Chouke et al., 1959). This result suggests instability for all wavelengths when the inequality

$$\frac{b^2 g \cos\theta}{12}(\rho_1 - \rho_2) - U(\mu_1 - \mu_2) > 0 \quad (3.8)$$

is satisfied, where g is the gravitational acceleration and θ is the fracture inclination with respect to the gravity vector. Although several assumptions have been made to derive this equation (e.g., that the fracture is smooth walled, fluids are incompressible, disturbances are infinitesimal, and capillary forces are negligible), the relationship between buoyant and viscous forces is instructive. Flows are seen to be either stabilized or destabilized by viscosity and density differences with the interfacial velocity modifying the viscosity difference. The role of capillarity at the interface has not been included in the derivation of Eq. 3.8; however, when it is included, it limits the unstable wavelengths to be above a minimum value. Most research has concentrated on viscous-driven fingering in smooth-walled fractures in the absence of gravity (see reviews by Saffman, 1986, and Homsy, 1987). Gravity-driven fingering has been studied recently in rough-walled analog fractures for air/water systems (Nicholl et al., 1992, 1993a,b; see Appendix 3.B).

Flow pulsation and/or blob flow has been noted in several experiments in transparent analog fractures. Pulsation was observed to be a function of flow rate during relative permeability experiments (Persoff et al., 1991). Flow pulsation and blob flow also have been documented to occur as flow rate through a stable gravity-driven finger is reduced (Nicholl et al., 1993b). In both of these situations, local interactions of the wetting and nonwetting fluids yield system dynamics that have the potential to be chaotic (see Appendixes 3.B and 3.C).

SEISMIC PROPERTIES

The two properties that characterize seismic wave propagation in all media are velocity and attenuation. Velocity is a function of the elastic moduli and density of the medium. Attenuation is a measure of the energy lost from the wave as it propagates. In general, fractures cause a decrease of the modulus of elasticity of the rock and hence a reduction in seismic velocity. They also cause energy loss, leading to increased attenuation. The physical processes governing both effects are discussed in the following sections. In most applications the seismic wavelength is large compared to fracture size (areal extent) and spacing, so the effects of individual fractures are embedded in parameters describing the bulk material behavior. These effective media models are discussed in the next section. More recently, the effects of individual fractures have been modeled explicitly, as discussed later in this chapter under "Discrete Fracture Effects."

APPENDIX 3.B
GRAVITY-DRIVEN INFILTRATION FLOW INSTABILITY

Consider a rock unit containing extensive, initially dry, inclined fractures that outcrop at the surface. A typical fluid source for infiltration into such fractures is surface ponding resulting from a locally intense rainfall event. Preferential flow associated with local fracture heterogeneity or differential supply of fluid will introduce finite-amplitude perturbations to the infiltration front, as shown in Figure 3.B1 for a transparent analog system. The driving force in the advancing front is the sum of gravitational (∇_g) and capillary (∇_c) gradients. Assuming that

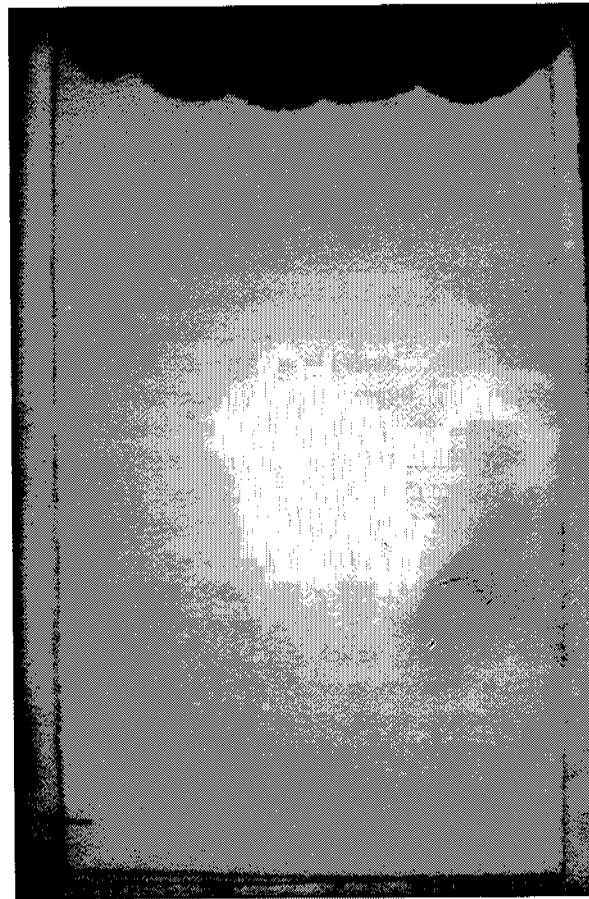


FIGURE 3.B1 Stable infiltration front initiated from application of a finite slug of fluid (black) into an initially dry fracture (white). Note that there are five significant perturbations to the front. From Nicholl et al. (1993b).

air (ψ_a) and water (ψ_w) entry pressure heads are independent of flow velocity, ∇_c can be approximated as

$$\nabla_c \approx \frac{\psi_a - \psi_w}{L_f} \quad (\text{B1})$$

where L_f describes the down-gradient length of the connected fluid column (Nicholl et al., 1992). During the initial stage of infiltration, fluid is freely available to the fracture; hence, no drainage behind the front occurs ($\psi_a = 0$) and capillary forces act to reinforce flow ($\nabla_c > 0$). Preferential flow occurs to regions of small L_f , thereby damping the initial finite-amplitude perturbations and stabilizing the front.

If fluid supply to the fracture is interrupted (i.e., the fluid supply becomes exhausted), the front can only advance by draining pores along its trailing edge. The introduction of a drainage pressure ($\psi_a < 0$) causes ∇_c to reverse direction and oppose flow. As a result, flow to the front is redistributed from regions of small L_f (large ∇_c) to regions of large L_f (small ∇_c) that develop into fingers (Figure 3.B2). The unstable front therefore bypasses significant portions of the fracture plane, advancing farther and faster than would be expected for an equivalent uniform front. The velocity of individual fingers is a function of system hydraulic parameters, ∇_c and L_f (Nicholl et al., 1992). As a finger advances, it leaves a partially wetted region behind (Figure 3.B2). The consequent loss of fluid causes the finger to slow and eventually halt in the fracture. Individual fingers therefore terminate in a fluid cluster that is "frozen" in place by capillary forces.

An unstable front will bypass significant portions of the fracture plane. Consequently, the volume of rock brought into hydraulic communication by a single infiltration event will be larger than that expected for an equivalent uniform front. Furthermore, at times short with respect to matrix imbibition and evaporative redistribution, the wetted structure created by unstable infiltration will have a significant effect on subsequent fracture infiltration. Ensuing infiltration events will preferentially follow the existing wetted structure. As the flow path is prewetted, finger velocity is increased over that observed in a dry fracture and very little fluid is lost during passage (Nicholl et al., 1993a,b). In effect, virtually the entire volume of an infiltration event is applied to the frozen fluid clusters associated with the previous event, restarting their movement and providing a mechanism for rapid recharge and solute transport.

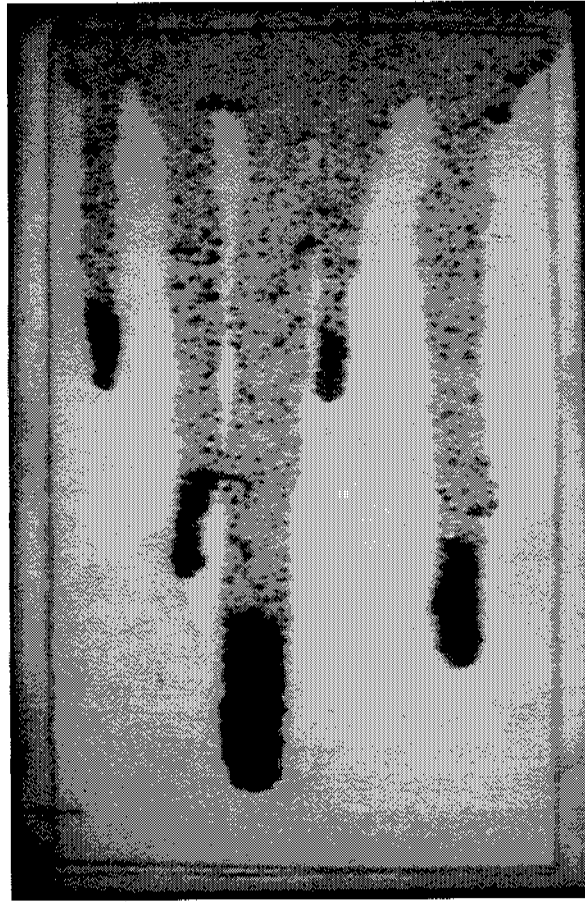


FIGURE 3.B2 Fingers originating from the stable front seen in Figure 3.B1. Partially saturated regions (mottled regions) are wetted near field capacity of the analog fracture. Courtesy of R. J. Glass.

APPENDIX 3.C
INFLUENCE OF TWO-PHASE STRUCTURE ON FRACTURE
PERMEABILITY AND SOLUTE TRANSPORT

Under steady-state conditions, flow in a single phase along the plane of a fracture is confined to the connected network of apertures filled by that phase. Decreasing phase saturation reduces the fraction of the fracture plane available for flow. The resultant decrease in cross-sectional area and increased flow tortuosity reduces the relative permeability for the phase.

Nicholl and Glass (1994) used a transparent analog rough-walled fracture to explore the effects of phase structure on fluid permeability and solute dispersion. Flow through the connected phase of a two-phase structure exhibited a channelization that was not observed under single-phase conditions (Figures 3.C1, 3.C2, and 3.C3). Path tortuosity of the channelized flow was observed to increase with complexity of the phase structure and size of the entrapped regions. Disconnected regions filled by the flowing phase are entirely isolated from flow under steady-state conditions. In addition, even in the connected regions, highly tortuous flow paths tend to bypass significant portions of the connected phase structure. This creates dead zones that do not actively participate in flow but communicate with active regions through diffusion. As a result, the average cross-sectional area of the connected phase structure is larger than the effective flow area.

For phase structures formed under nonequilibrium conditions, aperture filling may not follow a simple pressure/size relationship (Glass, 1993), further complicating the phase structure/permeability relationship. The fluid phase shown in Figure 3.C1 occupies 81.2 percent of the fracture plane. However, fluid permeability was only 14.3 percent of that measured at 100 percent saturation.

As expected from the previous discussion, two-phase wetted structure significantly affects solute dispersion. Flow channelization creates differential advection in the plane of the fracture (Figures 3.C2 and 3.C3). Velocity differentials introduced by local variations in cross-sectional area also act to increase dispersion. Dead zones created by flow tortuosity act to significantly extend the tail of the residence time distribution curve.

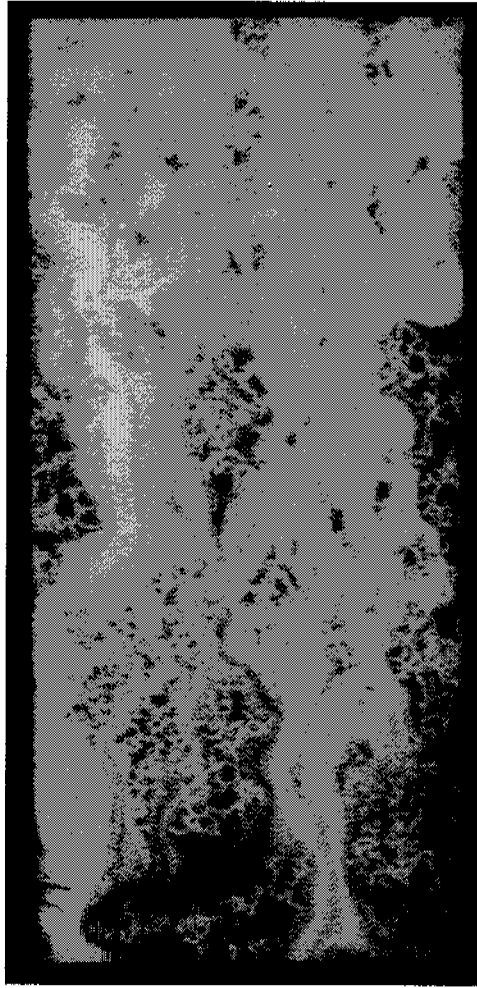


FIGURE 3.C1 Steady-state wetted structure in a transparent analog fracture. Dark areas are filled with dyed water; light regions are entrapped air. From Nicholl and Glass (1994).

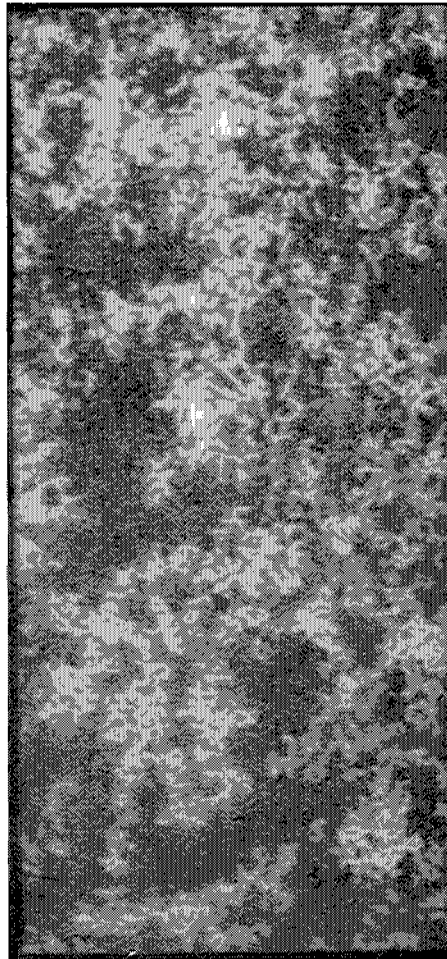


FIGURE 3.C2 Tracer pulse consisting of clear water entering the two-phase wetted structure in Figure 3.C1 from a constant flow boundary. From Nicholl and Glass (1994).

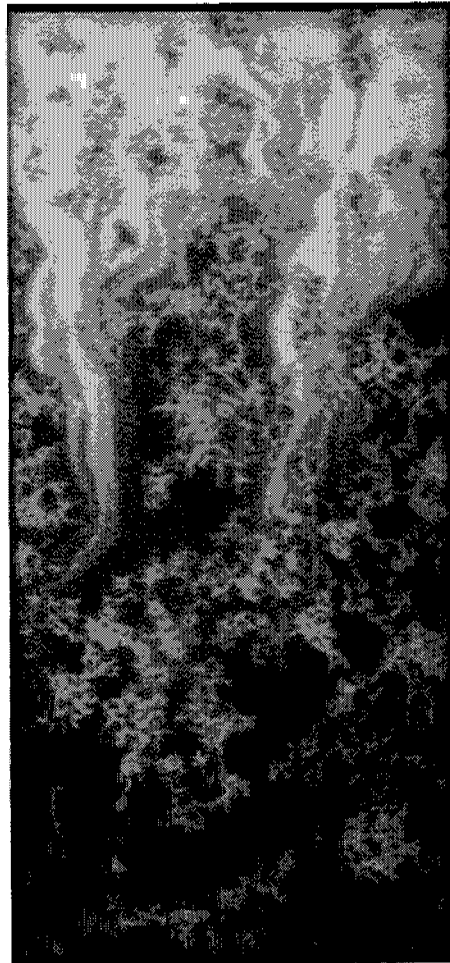


FIGURE 3.C3 Further development of the tracer pulse shown in Figure 3.C2. Note wholly isolated regions and dead zones that communicate by diffusion. From Nicholl and Glass (1994).